

Two-Dimensional Packing of Soft Particles and the Soft Generalized Thomson Problem

William L. Miller and Angelo Cacciuto*
Department of Chemistry, Columbia University
3000 Broadway, New York, New York 10027

We perform numerical simulations of purely repulsive soft colloidal particles interacting via a generalized elastic potential and constrained to a two-dimensional plane and to the surface of a spherical shell. For the planar case, we compute the phase diagram in terms of the system's rescaled density and temperature. We find that a large number of ordered phases becomes accessible at low temperatures as the density of the system increases, and we study systematically how structural variety depends on the functional shape of the pair potential. For the spherical case, we revisit the generalized Thomson problem for small numbers of particles $N \leq 12$ and identify, enumerate and compare the minimal energy polyhedra established by the location of the particles to those of the corresponding electrostatic system.

Introduction

Understanding how nanocomponents spontaneously organize into complex macroscopic structures is one of the great challenges in the field of soft matter today. Indeed, the ability to predict and control the phase behavior of a solution, given a set of components, may open the way to the development of materials with novel optical, mechanical, and electronic properties. Despite much effort in this direction, the question of how to link the physical character of the components, i.e. their bare shape and their interaction potential, to their phase behavior still remains unanswered.

Of particular interest for optical applications are the crystalline phases. Until recently, it was believed that shape anisotropy and/or directional interactions were key elements for the formation of crystals with complex symmetries commonly observed for instance in atomic solids. The study of the phase behavior of components interacting with exotic (yet isotropic) potentials has proven this belief to be incorrect. For instance, Torquato *et al.* have shown, using inverse optimization techniques, that it is possible to achieve non-closed-packed structures such as simple cubic, hexagonal, wurtzite and even diamond phases with isotropic pair potentials (see ref [1] for a review on the subject). Furthermore, spherical particles interacting via a hard core and a repulsive shoulder potential are known to organize into complex mesophases not unlike those found with diblock copolymers [2].

One class of pair potentials that has recently attracted much attention is that describing the interactions between soft/deformable mesoparticles. Unlike typical colloidal particles for which excluded volume interactions are strictly enforced via a hard-core or a Lennard-Jones potential, complex mesoparticles such as charged or neutral star polymers, dendrimers or microgels present a more peculiar pair potential describing their volume in-

teractions. Surprisingly, the simple relaxation of the constraint of mutual impenetrability between isotropic components gives access to several non-close-packed crystalline structures at high densities. Given the complexity of these mesoparticles, their interactions are usually extracted via an explicit coarse-grained procedure to obtain ad-hoc effective pair potentials. What emerges is a great variety of nontrivial interactions, some of which allow for even complete overlap among the components, resulting in a very rich phenomenological behavior. Remarkably, it is feasible to engineer interactions between star polymers or dendrimers by controlling their overall chemical/topological properties [3].

The phase behavior of several systems adopting these exotic, but physically inspired, interactions has been the subject of several publications [4–14]. Notably, it was found that some classes of soft interactions lead to reentrant melting transitions, others to polymorphic cluster phases [15], and in general to multiple transitions involving close-packed and non-close-packed crystalline phases [16–18] as a function of the system density. Remarkably, the phase behavior of these systems is very much dependent on the the shape of the pair potential. Likos *et al.* [19] established a criterion to predict whether for a bounded and repulsive potential reentrant melting or cluster phases will occur based on the sign of the Fourier transform of the interaction. Nevertheless, there is currently no method to predict *a priori* what specific crystal structures may become accessible for a given potential. For a recent review on the subject we refer the reader to reference [20].

In this paper we focus on two-dimensional systems. Although much of the research in this field has focused on three-dimensional systems, earlier numerical work on particles interacting via a hard core plus a shoulder potential in two dimensions has revealed a phenomenological behavior that can be as rich as that observed at higher dimensionality [21–24]. Here we focus on bounded soft potentials. Specifically, expanding on our recent results on Hertzian spheres [18] and dumbbells [25] in three dimensions, we analyze the phase behavior of soft elastic

*Electronic address: ac2822@columbia.edu

particles in two dimensions. We generalize our results to spherical surfaces, and discuss the generalized Thomson problem for our soft potentials by identifying novel polyhedral structures representing minimal energy configurations formed by soft particles constrained on the surface of a sphere at different packing densities.

Methods

To study the phase behavior of soft nanoparticles in two dimensions we performed numerical simulations. We considered systems of at least $N = 1000$ spherical particles and used the standard Monte Carlo method in the NPT and NVT ensemble for the planar and spherical case respectively. All simulations were run for a minimum of 10^6 iterations. Any two particles in our system interact via a Hertz potential. The Hertz potential describes the elastic energy penalty associated with an axial compression of two deformable spheres. Its functional form can be generalized as follows

$$V(r) = \begin{cases} \varepsilon(1 - \frac{r}{\sigma})^\alpha & \text{for } r \leq \sigma \\ 0 & \text{for } r > \sigma \end{cases} \quad (1)$$

where σ is the particle diameter, r is the interparticle distance, ε is the unit of energy, and α is a parameter that we control to modulate the shape of the interaction. The elastic case is recovered for $\alpha = 5/2$.

The Hertz model, developed to account for small elastic deformations, becomes inaccurate when associated to the large overlaps among particles that is achieved at large densities; nevertheless, it provides us with a simple representation of a finite-ranged, bounded soft potential with a positive definite Fourier transform (a condition that guarantees reentrant melting in the phase diagram.) We included in our study two more values of α to account for a slightly harder ($\alpha = 3/2$) and a slightly weaker ($\alpha = 7/2$) potential than the elastic one ($\alpha = 5/2$.) Figure 1 shows these potentials.

Crystallization in our simulations was determined using a combination of visual inspection and numerical order parameters similar to those described in [26]. Specifically, given a randomly chosen particle j , and a reference direction set to be along the bond between this particle and one of its nearest neighbors, we can define an order parameter sensitive to a crystal of D -fold symmetry (specifically six-fold hexagonal and four-fold square crystals) as follows: For all particles k within a radius of some cutoff r_c of j (including j itself), we calculate the angle ϕ_{lk} between the bond joining each of the D nearest neighbors l of k to k and the reference direction. If the number of particles within r_c of j is N_k , then the order parameter Ψ_D^j is given by: This process is then repeated N times and an average Ψ_D is calculated, yielding a value between 0 (for completely disordered systems) and 1 (for perfectly crystalline systems). This order parameter is analogous to that defined in [26] except that instead of

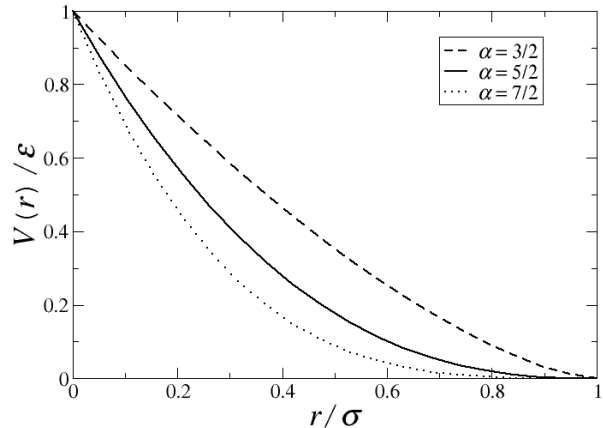


FIG. 1: Plot of the rescaled pair potential $V(r)/\varepsilon = (1 - \frac{r}{\sigma})^\alpha$ for the three values of α used in this study: $\alpha = \{\frac{3}{2}, \frac{5}{2}, \frac{7}{2}\}$

Ψ_D^i being an average over all particles k in the system, it is only over particles k within r_c ($= 1.65\sigma$ in our case); thus it is “semi-local” and allows crystalline order to be detected even in the presence of metastable grain boundaries. The order parameter in [26] represents the $r_c \rightarrow \infty$ limit of the above method.

To draw the phase diagrams we scan the phase space defined by the rescaled temperature $T_r = k_B T / \varepsilon$ and the rescaled number density $\rho_r = N\sigma^2/A$ (where A is the area of the system) to evaluate the several phases of the system in terms (when possible) of its order parameter Ψ_D . The lines separating the different regions are guides to the eye. Given the peculiarities of phase transitions in two dimensions, and the richness in the phases behavior reported, we have not attempted to establish equilibrium boundaries between the different phases, yet we have reproduced our results using Molecular Dynamics simulations with a Langevin Thermostat performed in key regions of the phase space, and compared the stability of the crystalline structures by measuring their relative energies at $T_r \rightarrow 0$.

Results

We begin by presenting the phase diagram for the case of Hertzian (elastic) spheres. The result is shown in Fig. 2. The labels in the figure refer to the structures shown in Fig. 4. As expected from Likos’s criterion [19] our system shows reentrant melting behavior and a highest temperature above which the system remains fluid at all densities.

The phase behavior here reported is qualitatively similar to that observed in three dimensions, however the two-dimensional system does not produce a phase space

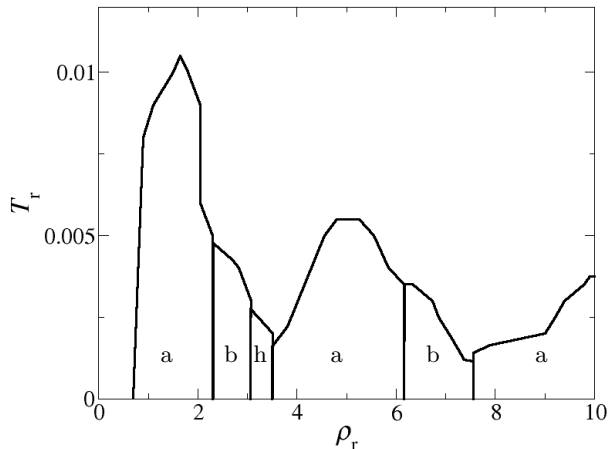


FIG. 2: Temperature vs. number density phase diagrams for two-dimensional particles interacting via a Hertz potential ($\alpha = 5/2$). Labels on the plots refer to the labels of the phases in Fig. 4.

that is as structurally rich as its three dimensional counterpart. Across the spectrum of densities (up to $\rho_r = 10$) and temperatures (down to $T_r = 10^{-6}$) that we explored, we find multiple crystal-to-crystal transitions from hexagonal (phase a) to square symmetry (phase b). Interestingly, the occurrence of the two phases has an alternating periodic pattern, and no isostructural transition was detected in our system [27].

This pattern is only broken at a small range of densities centered around $\rho_r \simeq 3.25$. This region (phase h) is characterized by a complex structure dominated by particles arranged mostly into pentagonal units. Our color coding of the phase shown in Fig. 4(h) helps rationalizing the overall symmetry of the structure which in this representation can be thought of as the combination of four square lattices. Three lattices are generated by pentagonal units, displaced with respect to each other but oriented along the same axis. The fourth lattice is built out of the non-connected particles and is oriented along an axis that forms an angle of 45 degrees with the other lattices.

To understand how the phase behavior is affected by the specific choice of the functional form of the potential, we repeated the calculation of the phase diagram for $\alpha = 7/2$ and $\alpha = 3/2$. The results are presented in Fig. 3. Although the overall trend is very similar, the number and the sequence of phases that we find are significantly different. Namely, $\alpha = 3/2$ leads to a significantly richer structural behavior, while the large value of α results in a single hexagonal crystalline structure. As a reference, notice that our potential tends to the linear-ramp potential for $\alpha = 1$ (for which a large number of phases including quasi-crystals have been observed [23]), we recover the square-shoulder potential for $\alpha \rightarrow 0$ (for which a cascade of cluster phases are expected), and tends to a Kronecker delta potential for $\alpha \rightarrow \infty$ (for which no crystallization

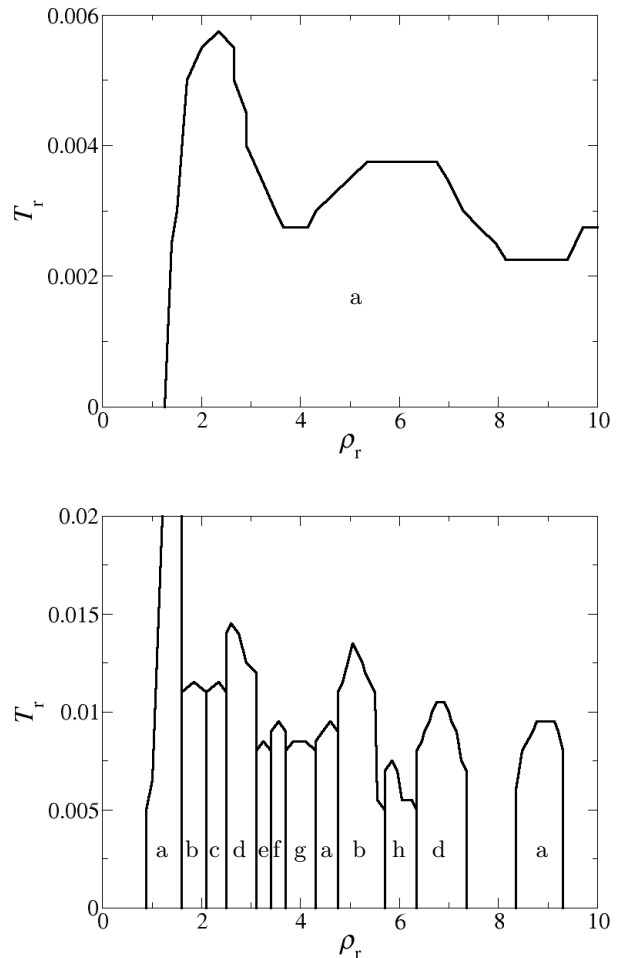


FIG. 3: Temperature vs. number density phase diagrams for two-dimensional particles interacting via the generalized Hertz potential with $\alpha = 7/2$ (top) and $\alpha = 3/2$ (bottom). Labels on the plots refer to the labels of the phases in Fig. 4.

is expected at any finite density).

At least as a general trend, it is therefore not surprising that structural variety increases for smaller values of α . In this regard, it is interesting to estimate the critical power above which the hexagonal lattice becomes the only stable lattice as observed in Fig. 3(bottom). Given that the only other competing structure at large values of α is the square lattice, we computed the energy density difference between hexagonal and square lattices as a function of density and at zero temperature for different values of α . The result is presented in Fig. 5 for densities up to $\rho_r = 25$ (our full numerical data extend up to $\rho_r = 100$, but are not shown for the sake of clarity). We find that the hexagonal lattice becomes more stable than the square lattice at all densities for any powers above the onset value $\alpha^* \simeq 3.182$. Several numerical simulations at finite densities for powers ranging from $\alpha = 10$ to $\alpha = 50$ were carried out, and indeed only hexagonal structures

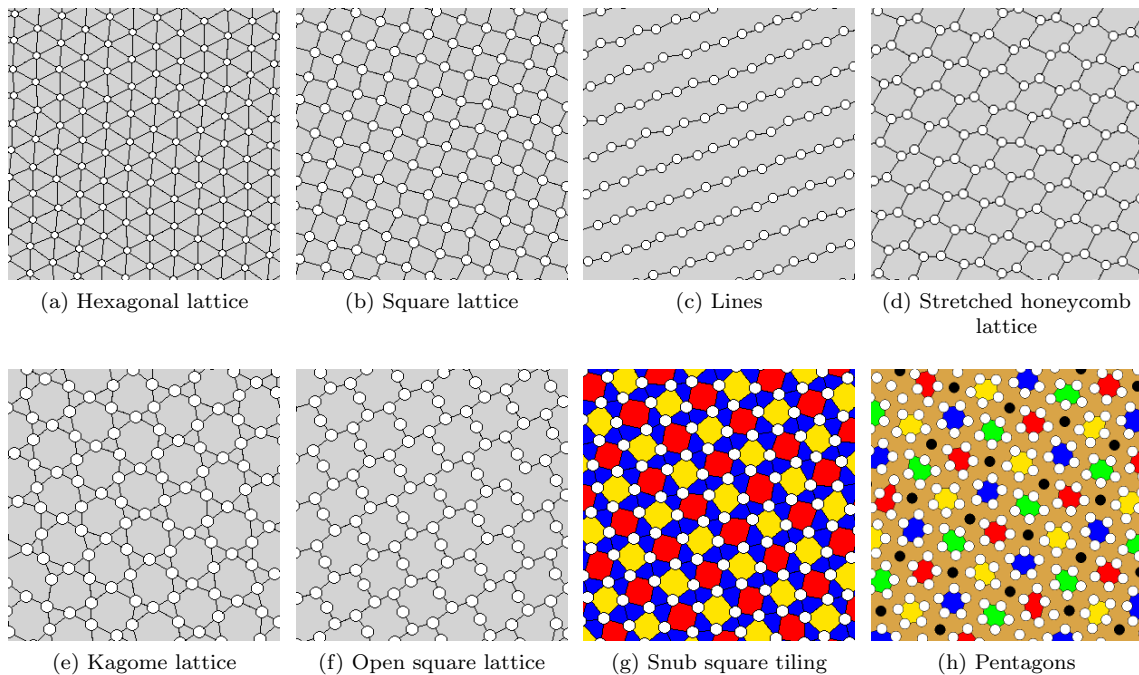


FIG. 4: Two-dimensional crystal phases formed in these systems.

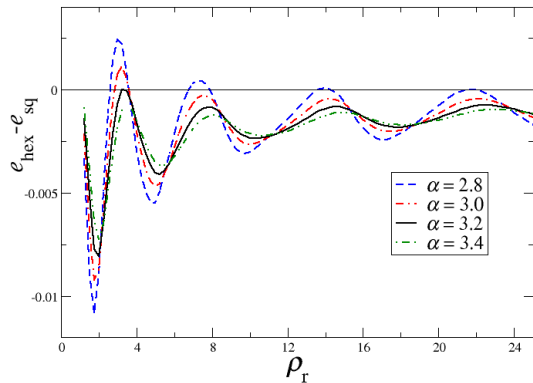


FIG. 5: Energy density difference between hexagonal and square lattice at $T_r = 0$ as a function of system density at different values of α . We estimated the critical α to be around $\alpha \simeq 3.1822$.

where observed upon system ordering. The presence of reentrant melting was also established for $\alpha = 5$ and $\alpha = 10$. The oscillating behavior of the energy density difference for $\alpha < \alpha^*$ also explains qualitatively the periodic structural pattern observed in the phase diagram for $\alpha = 5/2$.

We now turn to the discussion of the second part of the paper. Given the structural variety observed in the two dimensional compression of soft nanoparticles,

it is interesting to extend our results to other geometries. The spherical case is of particular interest because a large body of work has been dedicated to finding and enumerating minimal energy conformations of particles constrained over a spherical shell, and repelling each other via an electrostatic repulsion [28–39]. This is what Thomson asked in 1904 [40] when attempting to construct his plum pudding model of the atom. Although there is consensus on the minimal energy structures for $N < 100$, the problem becomes more involved for large values of N for which an exponentially large number of low energy configurations becomes available. In this regime, lattices with overall icosahedral symmetry (*icosadeltahedra*) have been initially postulated as possible global minima for specific magic number of particles [34], but eventually it was shown that it is possible to lower the energy of these configurations adding dislocation defects [37, 41]. Grain boundary scars have also been observed in experiments [42].

Although we confirm that the same pattern of phases obtained in two dimensions also develops on large areas of spherical shells – apart from the topologically required defects – as a function of the radius of the sphere (see Fig. 6 for a sample of these configurations), we have not attempted to enumerate all possible low energy states for large N . It is however clear that considering soft potentials introduces two new parameters to the system: namely the packing density and the shape of the potential. A careful analysis of the defects and symmetries arising in this regime is currently under investigation and will be the subject of another publication; here we focus on the case of small number of particles $N \leq 12$ for

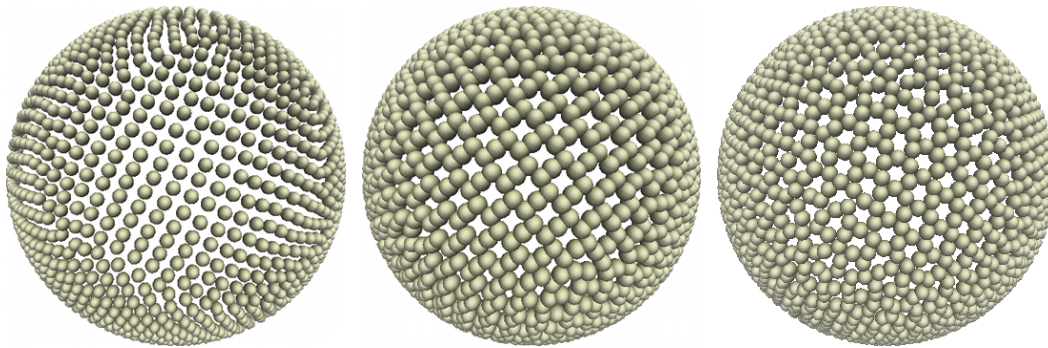


FIG. 6: Snapshots of soft particles packing on a spherical surface. Here we show from left to right square, open square and kagome lattices.

$\alpha = 3/2$ and $\alpha = 5/2$.

Figures 7 and 8 show the results of our analysis for $N \in \{5, 12\}$. The rescaled configurational energy E defined as the total internal energy divided by ε , the reduced radius $r_0 = R/\sigma$ of the spherical surface and the names of the polyhedra (when available) are also given. The reference configurations for the electrostatic problem are highlighted with a dark frame. These data are obtained using both Monte Carlo and Molecular Dynamics simulations with a standard temperature annealing procedure down to $T_r \rightarrow 0$.

Unlike the case of charged point particles, we find that indeed the number and the nature of the structures is very much dependent on the radius of the sphere. The overall trend follows what found in the analysis of the planar two-dimensional system; namely, smaller values of α lead to richer structural diversity. In all cases we were able to recover the global minima of the electrostatic system for at least one spherical radius. Interestingly, $N = 4$ and $N = 6$ are the only cases in which for both powers we obtain only one structure, a tetrahedron and an octahedron respectively (not shown), which are stable for any value of r_0 explored (down to $r_0 = 0.10$). The stability of the octahedron ($N = 6$) was also confirmed for values of α up to 10. Low energy configurations for values of N larger than 12 have also been considered, however, given the large variety and the complexity of the structures arising upon increasing N , we have not attempted to enumerate them. In fact, more sophisticated algorithms than the one used in this work would be necessary to thoroughly explore the energy landscape in search of a global minimum.

Conclusions

In this paper we explore the phase behavior of colloidal particles interacting via a generalized soft (Hertz) potential. Specifically, we analyze how structural diversity depends on the particular choice of the functional form of the potential for particles constrained on a two-

dimensional plane and on the surface of a spherical shell. For the planar case we compute how the phase diagram of the system changes with the functional form of the pair potential, and establish a limit above which (for the class of potentials explored) hexagonal packing becomes the only allowed symmetry of the ordered phase. For small number of particles ($N \leq 12$), we identify on a spherical shell the polyhedral configurations establishing global energy minima for different pair potentials, and compare the results to the global minima corresponding to the classic Thomson problem. We show that unlike the electrostatic case, for the same number of particles the system presents more than one global minimum depending on the radius of the sphere.

It would be interesting to study the geometry of the defects arising for larger number of particles on the spherical shell, analyze the overall symmetry of the ground states, and explore whether patterns of grain boundaries, expected for large values of N in the electrostatic system, would also manifest for soft potentials. This is a very challenging problem that we have already begun to investigate and requires more sophisticated minimization techniques than the ones employed in this study. For the time being, we have established that the same phases observed in the planar geometry do develop on the spherical shell at comparable number densities.

Finally, given the sensitivity of the phase behavior on the specific choice of the pair potential, it becomes critical at this point to develop sophisticated and reliable coarse-graining procedures able to capture accurate interactions between dendrimers or star polymers, but also the inverse problem, i.e. the design of polymeric structures able to reproduce desired functional forms for the pair potential, is in great need of a better theoretical understanding.

ACKNOWLEDGMENTS

This work was supported by the American Chemical Society under PRF grant No. 50221-DNI6 A. C. thanks Vincent Nguyen for helping with the simulations.

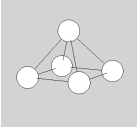
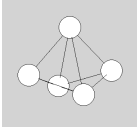
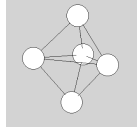
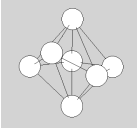
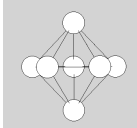
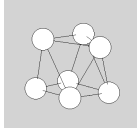
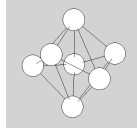
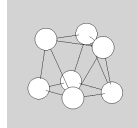
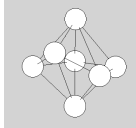
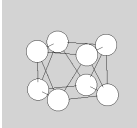
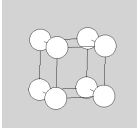
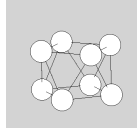
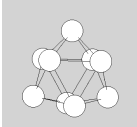
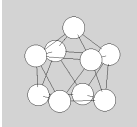
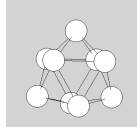
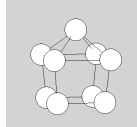
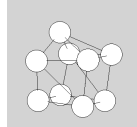
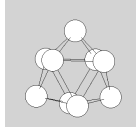
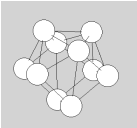
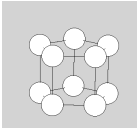
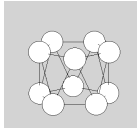
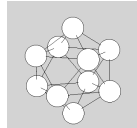
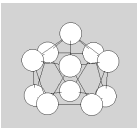
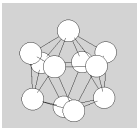
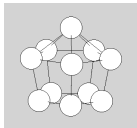
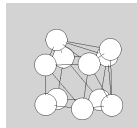
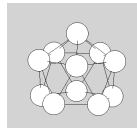
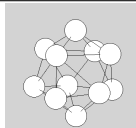
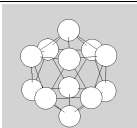
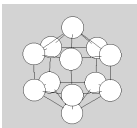
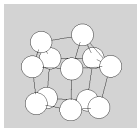
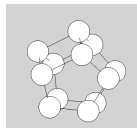
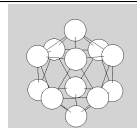
N_b	Cluster geometry					
5	 square pyramid $r_0 = 0.65$ $E = 0.116675$	 $P_A^{(5)}$ $r_0 = 0.58$ $E = 0.457195$	 trigonal dipyramid $r_0 = 0.50$ $E = 1.098194$			
7	 $P_A^{(7)}$ $r_0 = 0.75$ $E = 0.1481239$	 pentagonal dipyramid $r_0 = 0.65$ $E = 0.802319$	 $P_B^{(7)}$ $r_0 = 0.58$ $E = 1.635489$	 $P_C^{(7)}$ $r_0 = 0.55$ $E = 2.066014$	 $P_B^{(7)}$ $r_0 = 0.50$ $E = 2.956885$	 $P_A^{(7)}$ $r_0 = 0.40$ $E = 5.463620$
8	 square antiprism $r_0 = 0.70$ $E = 0.851626$	 cube $r_0 = 0.58$ $E = 2.423538$	 square antiprism $r_0 = 0.50$ $E = 4.212084$			
9	 triaugmented triangular prism $r_0 = 0.81$ $E = 0.268064$	 gyroelongated square pyramid $r_0 = 0.78$ $E = 0.508830$	 triaugmented triangular prism $r_0 = 0.70$ $E = 1.424194$	 elongated square pyramid $r_0 = 0.63$ $E = 2.489422$	 $P_A^{(9)}$ $r_0 = 0.58$ $E = 3.479048$	 triaugmented triangular prism $r_0 = 0.50$ $E = 5.696124$
10	 sphenocorona $r_0 = 0.90$ $E = 0.035971$	 pentagonal prism $r_0 = 0.60$ $E = 4.102489$	 pentagonal antiprism $r_0 = 0.57$ $E = 4.921405$	 gyroelongated square dipyramid $r_0 = 0.40$ $E = 12.689921$		
11	 gyroelongated pentagonal pyramid $r_0 = 0.90$ $E = 0.244728$	 $P_A^{(11)}$ $r_0 = 0.80$ $E = 1.308288$	 elongated pentagonal pyramid $r_0 = 0.68$ $E = 3.322424$	 $P_B^{(11)}$ $r_0 = 0.63$ $E = 4.479854$	 gyroelongated pentagonal pyramid $r_0 = 0.55$ $E = 7.042131$	 $P_C^{(11)}$ $r_0 = 0.40$ $E = 15.783736$
12	 icosahedron $r_0 = 0.90$ $E = 0.373165$	 elongated pentagonal dipyramid $r_0 = 0.75$ $E = 2.857171$	 $P_A^{(12)}$ $r_0 = 0.70$ $E = 3.806734$	 $P_B^{(12)}$ $r_0 = 0.65$ $E = 5.087802$	 icosahedron $r_0 = 0.50$ $E = 11.529991$	

FIG. 7: Global minimum configurations formed by small number of particles constrained on the surface of a sphere interacting with a generalized hertzian soft potential for $\alpha = 3/2$, at different values of reduced sphere radius r_0 .

The reduced energy of the configurations is also indicated together with the name of the polyhedral structures.

Some structures for which no name was found are indicated with the nomenclature $P_X^{(N)}$. For $N = 4$ and $N = 6$ (not shown) we obtain respectively a tetrahedral and an octahedral structure for every r_0 . Reference configurations for long-range potentials have been highlighted with a dark border.

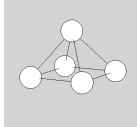
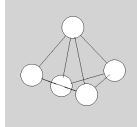
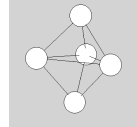
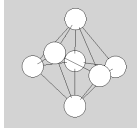
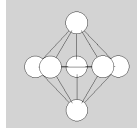
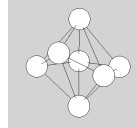
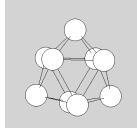
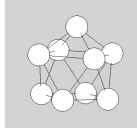
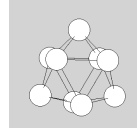
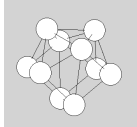
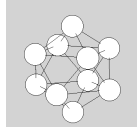
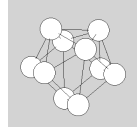
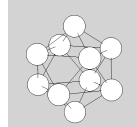
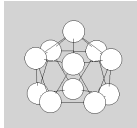
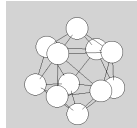
N_b	Cluster geometry			
5	 square pyramid $r_0 = 0.70$ $E = 0.000047$	 $P_A^{(5)}$ $r_0 = 0.58$ $E = 0.081254$	 trigonal dipyramid $r_0 = 0.50$ $E = 0.298277$	
7	 $P_A^{(7)}$ $r_0 = 0.75$ $E = 0.008832$	 pentagonal dipyramid $r_0 = 0.50$ $E = 1.012408$	 $P_A^{(7)}$ $r_0 = 0.25$ $E = 6.627468$	
9	 triaugmented triangular prism $r_0 = 0.75$ $E = 0.110712$	 gyroelongated square pyramid $r_0 = 0.72$ $E = 0.196371$	 triaugmented triangular prism $r_0 = 0.50$ $E = 2.203406$	
10	 sphenocorona $r_0 = 0.80$ $E = 0.097219$	 gyroelongated square dipyramid $r_0 = 0.65$ $E = 0.850254$	 sphenocorona $r_0 = 0.60$ $E = 1.361079$	 gyroelongated square dipyramid $r_0 = 0.50$ $E = 2.986067$
11	 gyroelongated pentagonal pyramid $r_0 = 0.80$ $E = 0.221753$	 $P_A^{(11)}$ $r_0 = 0.70$ $E = 0.793120$		

FIG. 8: Global minima configurations formed by small number of particles constrained on the surface of a sphere interacting with a generalized hertzian soft potential for $\alpha = 5/2$, at different values of reduced sphere radius r_0 .

The reduced energy of the configurations is also indicated together with the name of the polyhedral structures. Some structures for which no name was found are indicated with the nomenclature $P_X^{(N)}$. For $N = 4$, $N = 6$ and $N = 12$ (not shown) we obtain respectively a tetrahedral, an octahedral and an icosahedral structure for every r_0 .

Reference configurations for long-range potentials have been highlighted with a dark border.

-
- [1] S. Torquato, *Soft Matter* **5**, 1157 (2009).
[2] M. Glaser, G. Grason, R. Kamien, A. Kovsmrlj, C. Santangelo, and P. Zihler, *Europhysics Lett.* **78**, 46004 (2007).
[3] B. M. Mladek, H. Kahl, and C. N. Likos, *Phys. Rev. Lett.* **100**, 028301 (2008).
[4] A. A. Louis, P. G. Bolhuis, J. P. Hansen, and E. J. Meijer, *Phys. Rev. Lett.* **85**, 2522 (2000).
[5] O. Götze, H. M. Harreis, and C. N. Likos, *J. Chem. Phys.* **120**, 7761 (2004).
[6] C. N. Likos, H. L. Watzlawek, B. Abbas, O. Jucknischke, J. Allgaier, and D. Richter, *Phys. Rev. Lett.* **80**, 4450 (1998).
[7] A. Jusufi, C. N. Likos, and H. Löwen, *Phys. Rev. Lett.* **88**, 018301 (2002).
[8] A. R. Denton, *Phys. Rev. E* **67**, 11804 (2003).
[9] D. Gottwald, C. N. Likos, G. Kahl, and H. Löwen, *Phys. Rev. Lett.* **92**, 68301 (2004).

- [10] C. Pierleoni, C. Addison, J. P. Hansen, and V. Krakoviack, Phys. Rev. Lett. **96**, 128302 (2006).
- [11] B. Capone et al., J. Phys. Chem. B **113**, 3629 (2008).
- [12] B. Bozorgui, M. Sen, W. L. Miller, J. C. Pámies, and A. Cacciuto, J. Chem. Phys. **132**, 014901 (2010).
- [13] C. Zhao, K. Tian, and N. Xu, Phys. Rev. Lett. **106**, 125503 (2011).
- [14] S. Prestipino, F. Saija, and G. Malescio, Soft Matter **5**, 2795 (2009).
- [15] B. M. Mladek, D. Gottwald, G. Kahl, M. Neumann, and C. N. Likos, Phys. Rev. Lett. **96**, 045701 (2006).
- [16] A. Suto, Phys. Rev. B **74**, 104117 (2006).
- [17] C. N. Likos, Nature **440**, 433 (2006).
- [18] J. Pámies, A. Cacciuto, and D. Frenkel, J. Chem. Phys. **131**, 044514 (2009).
- [19] C. N. Likos, N. Hoffmann, and H. Löwen, Phys. Rev. E **63**, 031206 (2001).
- [20] C. N. Likos, Soft Matter **2**, 478 (2006).
- [21] G. Malescio and G. Pellicane, Nature Materials **2**, 97 (2003).
- [22] G. Stell and P. C. Hemmer, J. Chem. Phys. **56**, 4274 (1970).
- [23] E. A. Jagla, Phys. Rev. R **58**, 1478 (1998).
- [24] M. Glaser, private communication.
- [25] A. Šarić, B. Bozorgui, and A. Cacciuto, J. Phys. Chem. B **8**, 1 (2011).
- [26] K. Binder, S. Sengupta, and P. Nielaba, J. Phys.: Condens. Matter **14**, 2323 (2002).
- [27] K. Zhang, P. Charbonneau, and B. Mladek, Phys. Rev. Lett. **105**, 245701 (2010).
- [28] E. L. Altschuler, T. J. Williams, E. R. Ratner, F. Dowla, and F. Wooten, Phys. Rev. Lett. **72**, 2671 (1994).
- [29] T. Erber and G. M. Hockney, Phys. Rev. Lett. **74**, 1482 (1995).
- [30] A. Pérez-Garrido, M. O. no, E. Cuevas, and J. Ruiz, Journal of Physics A: Mathematical and General **29**, 1973 (1996).
- [31] J. R. Morris, D. M. Deaven, and K. M. Ho, Phys. Rev. B **53**, R1740 (1996).
- [32] T. Erber and G. M. Hockney, *Complex Systems: Equilibrium Configurations of N Equal Charges on a Sphere ($2 \leq N \leq 112$)* (John Wiley & Sons, Inc., 2007), pp. 495–594.
- [33] J. R. Edmundson, Acta Crystallographica Section A **49**, 648 (1993).
- [34] E. L. Altschuler, T. J. Williams, E. R. Ratner, R. Tipton, R. Stong, F. Dowla, and F. Wooten, Phys. Rev. Lett. **78**, 2681 (1997).
- [35] M. J. W. Dodgson and M. A. Moore, Phys. Rev. B **55**, 3816 (1997).
- [36] A. Pérez-Garrido, M. J. W. Dodgson, M. A. Moore, M. Ortuño, and A. Díaz-Sánchez, Phys. Rev. Lett. **79**, 1417 (1997).
- [37] A. Pérez-Garrido, M. J. W. Dodgson, and M. A. Moore, Phys. Rev. B **56**, 3640 (1997).
- [38] M. J. Bowick, A. Cacciuto, D. R. Nelson, and A. Travesset, Phys. Rev. B **73**, 024115 (2006).
- [39] M. J. Bowick, A. Cacciuto, D. R. Nelson, and A. Travesset, Phys. Rev. Lett. **89**, 185502 (2002).
- [40] J. J. Thomson, Philos. Mag. **7**, 237 (1904).
- [41] M. J. Bowick, D. R. Nelson, and A. Travesset, Phys. Rev. B **62**, 8738 (2000).
- [42] A. R. Bausch, M. J. Bowick, A. Cacciuto, A. D. Dinsmore, F. Hsu, D. R. Nelson, M. G. Nikolaides, A. Travesset, and D. A. Weitz, Science **299**, 1716 (2003).